Evolution of magnetism in single-crystal $Ca_2Ru_{1-x}Ir_xO_4$ ($0 \leqslant x \leqslant 0.65$)

S. J. Yuan,[1,*] J. Terzic,[1] J. C. Wang,[1,2,3] L. Li,[1] S. Aswartham,[1] W. H. Song,[1,4] F. Ye,[2] and G. Cao[1,†]

[1]*Center for Advanced Materials, Department of Physics and Astronomy, University of Kentucky, Lexington, Kentucky 40506, USA*

[2]*Quantum Condensed Matter Division, Oak Ridge National Laboratory, Oak Ridge, Tennessee 37831, USA*

[3]*Department of Physics, Renmin University of China, Beijing 100872, China*

[4]*Institute of Solid State Physics, Chinese Academy of Sciences, Hefei 230031, China*

(Received 7 April 2015; published 24 July 2015)

We report structural, magnetic, transport, and thermal properties of single-crystal $Ca_2Ru_{1-x}Ir_xO_4$ ($0 \leqslant x \leqslant 0.65$). Ca_2RuO_4 is a structurally driven Mott insulator with a metal-insulator transition at $T_{MI} = 357$ K, which is well separated from antiferromagnetic order at $T_N = 110$ K. Substitution of a 5*d* element, Ir, for Ru enhances spin-orbit coupling and locking between the structural distortions and magnetic moment canting. Ir doping intensifies the distortion or rotation of Ru/IrO_6 octahedra and induces weak ferromagnetic behavior along the *c* axis. In particular, Ir doping suppresses T_N but concurrently causes an additional magnetic ordering T_{N2} at a higher temperature up to 210 K for $x = 0.65$. The effect of Ir doping sharply contrasts with that of 3*d*-element doping such as Cr, Mn, and Fe, which suppresses T_N and induces unusual negative volume thermal expansion. The stark difference between 3*d*- and 5*d*-element doping underlines a strong magnetoelastic coupling inherent in the Ir-rich oxides.

DOI: 10.1103/PhysRevB.92.024425 PACS number(s): 71.70.Ej, 75.30.Kz, 71.30.+h

I. INTRODUCTION

The Coulomb interaction U is generally comparable to the 4*d* bandwidth W in the 4*d*-based ruthenates, which leaves them precariously balanced on the border between metallic and insulating behavior, or on the verge of long-range magnetic order. A common characteristic of these materials is that underlying physical properties are critically linked to the lattice and orbital degrees of freedom and tend to exhibit a giant response to modest lattice changes. This is dramatically illustrated by Sr_2RuO_4 and Ca_2RuO_4, where the former compound exhibits a prototypical *p*-wave superconducting state [1] that strongly contrasts with the more distorted structure (due to a smaller ionic radius $r_{Ca} < r_{Sr}$) and first-order metal-insulator transition, T_{MI}, observed for the latter compound [2,3].

Extensive investigations of Ca_2RuO_4 [4,5] have established that a strong cooperative Jahn-Teller distortion removes the degeneracy of the three Ru t_{2g} orbitals (d_{xy},d_{yz},d_{zx}) via a transition to orbital order that, in turn, drives the metal-insulator transition at $T_{MI} = 357$ K [6–14]. Classic Mott insulators undergo simultaneous transitions to antiferromagnetic (AFM) order and an insulating state at T_{MI}. However, Ca_2RuO_4 undergoes AFM order at $T_N = 110\,\text{K} \ll T_{MI}$ [2], and is therefore a highly interesting and unique archetype of a metal-insulator transition that is strongly coupled to a structural transition from a high-T tetragonal to low-T orthorhombic distortion and is not driven by AFM exchange interactions [2,3,6,12].

We recently observed that slight substitutions of a 3*d* element M(M = Cr,Mn,Fe) for Ru shifts T_{MI}, weakens the orthorhombic distortion, and induces either metamagnetism or magnetization reversal below T_N [12–14]. Furthermore, M doping for Ru produces substantial negative thermal expansion in $Ca_2Ru_{1-x}M_xO_4$, with a total volume expansion ratio $\Delta V/V$ as high as 1% on cooling. The onset of the negative thermal expansion closely tracks shifts of T_{MI} and T_N, and sharply contrasts with classic examples of negative thermal expansion that show no correlation with electronic properties. These unusual observations suggest a complex interplay between orbital, spin, and lattice degrees of freedom [12–14].

It is important to note Ru^{4+} ($4d^{4+}$) ions tend to adopt a low-spin state or $S = 1$ state because relatively large crystal fields often overpower the Hund's rule coupling [15]. On the other hand, the spin-orbit coupling (SOC) may be strong enough to impose a competing singlet, or an angular momentum, $J_{\text{eff}} = 0$, ground state [15,16]. Compared to 4*d* ruthenates, 5*d* iridates have stronger SOC (~0.4 eV, compared to ~0.16 eV for Ru ions) [17], which compete vigorously with Coulomb interactions, noncubic crystalline electric fields, and Hund's rule coupling [17–21]. A profound manifestation of this competition is the interesting "$J_{\text{eff}} = 1/2$ Mott state" that was recently observed in the layered iridates with tetravalent Ir^{4+} ($5d^{4+}$) ions [18,19]. Therefore, substitution of Ir for Ru in 4*d* ruthenates is expected to promote alternative magnetic behavior. Moreover, in light of the unique insulating state recently discovered in Sr_2IrO_4 [18], a comparison with its isostructural compound Ca_2IrO_4 would be desirable. However, the structural instability prevents the formation of the perovskitelike Ca_2IrO_4; the heavily Ir-doped Ca_2RuO_4 or $Ca_2Ru_{1-x}Ir_xO_4$ with x up to 0.65 thus provides an alternative for comparison and contrast to the archetype $J_{\text{eff}} = 1/2$ insulator Sr_2IrO_4 that antiferromagnetically orders at 240 K [22].

In this paper, we report results of our study of single-crystal $Ca_2Ru_{1-x}Ir_xO_4$ with $0 \leqslant x \leqslant 0.65$. Our central findings are that increasing Ir substitution suppresses T_N but simultaneously induces an additional magnetic order at a higher temperature, T_{N2}, which reaches as high as 210 K at $x = 0.65$. Ir doping also causes a dramatic increase in moment canting and the appearance of a weak ferromagnetic (FM) moment along the *c* axis, along with enhanced magnetic anisotropy due to increased SOC. The increase in both T_{N2} and T_{MI} with increased Ir doping closely follows the enhanced Ru/IrO_6

*shujuan.yuan@uky.edu

†cao@uky.edu

octahedral rotation or reduced Ru/Ir-O-Ru/Ir bond angle. This study reveals that Ir doping enhances the coupling between the lattice and magnetic moment, sharply contrasting 3*d*-element doping that readily reduces such a coupling and orthorhombic distortions; it thus suppresses the AFM and insulating states. The pronounced difference illustrated in this study highlights a strong magnetoelastic coupling inherent in the SOC-driven iridates that dictates magnetic properties. This work also provides an important comparison to the extensively studied Sr_2IrO_4.

II. EXPERIMENT

Single crystals were grown using flux techniques described elsewhere [23]. The structures of $Ca_2Ru_{1-x}Ir_xO_4$ were determined using a Nonius Kappa CCD x-ray diffractometer at 90 K. Structures were refined by full-matrix least squares using the SHELX-97 programs [24]. All structures affected by absorption and extinction were corrected by comparison of symmetry-equivalent reflections using the program SADABS [24]. It needs to be emphasized that the single crystals are of high quality and there is no indication of any mixed phases or inhomogeneity in the single crystals studied. The standard deviations of all lattice parameters and interatomic distances are smaller than 0.1%. More detailed information is available in the Supplemental Material (SM) [25]. Chemical compositions of the single crystals were estimated using both single-crystal x-ray diffraction and energy dispersive x-ray (EDX) analysis (Hitachi/Oxford 3000). Magnetization, specific heat, and electrical resistivity were measured using either a Quantum Design MPMS-7 SQUID Magnetometer and/or a Physical Property Measurement System with 14-T field capability.

III. RESULTS AND DISCUSSION

Ca_2RuO_4 adopts a very peculiar distortion of the K_2NiF_4 prototype with a *Pbca* (61) space group consisting of layers of RuO_6 octahedra separated by Ca atoms [4,14]. Neighboring corner-shared octahedra tilt and rotate in an ordered manner; as a result, the Ru-O-Ru bond angle is severely distorted from 180°.

Substituting Ir^{4+} for Ru^{4+} preserves the crystal structure but results in a reduction in the *a*- and *b*-axis lattice parameters and an elongation in the *c*-axis lattice parameter, and eventually shrinks the unit cell volume V, as shown in Fig. 1(a). Compared to the parent compound Ca_2RuO_4, the c/a ratio increases, by 1.9% for $x = 0.5$ at 90 K, for example. The orthorhombic distortion also increases with increasing x; e.g., $(b-a)/b = 0.0437465$ for $x = 0$, and $(b-a)/b = 0.0467$ for $x = 0.5$ at 90 K. The decrease in the bond angle Ru/Ir-O1-Ru/Ir, Θ, is a further manifestation of more distorted Ru/IrO_6 octahedra for the Ir-doped compounds, sharply contrasting with that for a 3*d*-element doping [12–14]. The decrease in Θ has important implications for magnetic and transport properties, as discussed below.

The magnetic susceptibility $\chi(T)$ of the parent compound Ca_2RuO_4 exhibits a sharp anomaly due to AFM ordering at $T_N = 110$ K [see inset in Fig. 2(a)] [2]. Ir doping induces pronounced changes in the magnetic properties of single-crystal $CaRu_{1-x}Ir_xO_4$, as shown in Fig. 2. It suppresses T_N but concurrently introduces an additional magnetic ordering T_{N2} at higher temperatures. For example, T_N decreases to 80 K at $x = 0.34$ from 110 K at $x = 0$; at the same time, T_{N2}

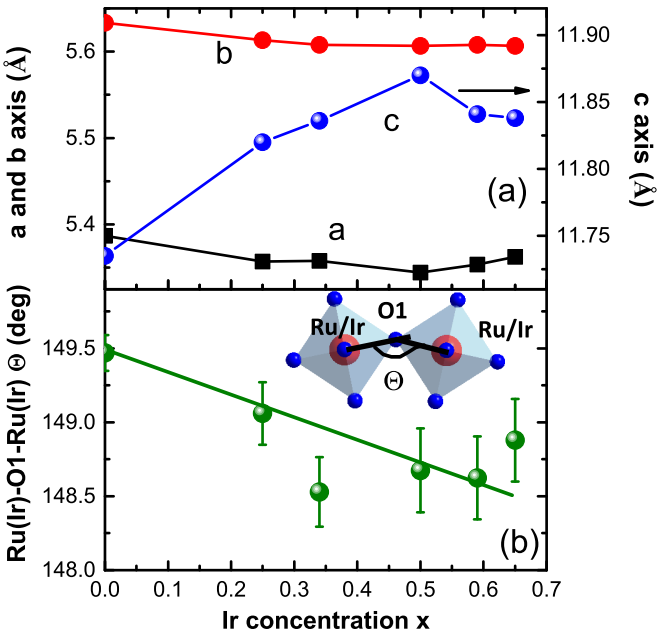

FIG. 1. (Color online) Ir concentration x dependence of (a) the *a*-, *b*-, and *c*-axis lattice parameters (right scale); and (b) Ru/Ir-O1-Ru/Ir bond angle Θ for $CaRu_{1-x}Ir_xO_4$ at $T = 90$ K. Inset: A schematics of the distorted Ru/Ir-O1-Ru/Ir bond angle Θ.

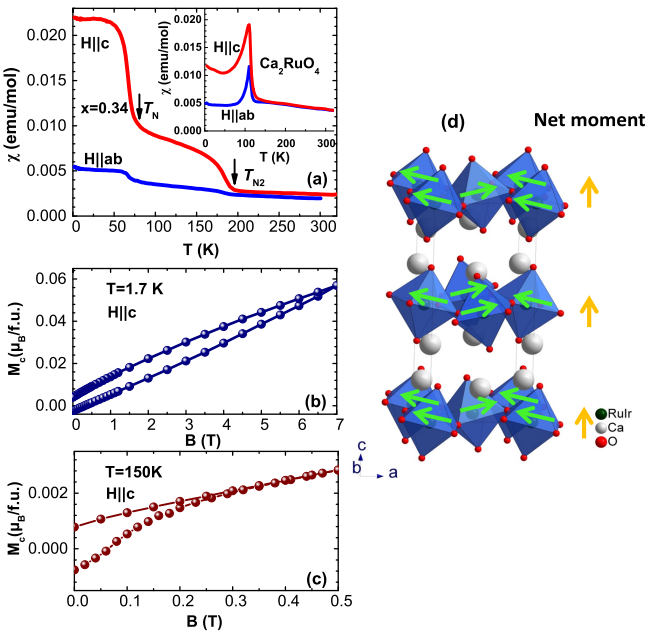

FIG. 2. (Color online) (a) Magnetic susceptibility $\chi(T)$ at $\mu_0 H = 0.1$ T, (b, c) the isothermal magnetization $M(H)$ at 1.7 and 150 K, respectively, for $x = 0.34$. The inset in (a) shows $\chi(T)$ for $x = 0$. The $\chi(T)$ data were measured under 0.1 T after field cooling (FC). The $M(H)$ were measured after a zero-field-cooled (ZFC) process. (d) The schematic of the magnetic structure derived from the magnetic results for $CaRu_{1-x}Ir_xO_4$.

emerges at 190 K, as shown in Fig. 2(a). T_{N2} signals a weak FM behavior along the c axis. The sizable hysteresis in isothermal magnetization along the c axis is consistent with the weak FM behavior, as shown in Figs. 2(b) and 2(c). Furthermore, there is a strong magnetic anisotropy that renders a much weaker magnetic response in the ab plane.

Ca_2RuO_4 has a canted AFM structure adapted to a Dzyaloshinskii-Moriya (DM) interaction on a distorted orthorhombic perovskite structure [14,26–29]. The spins are canted away from the ab plane toward the c axis; consequently the value of the susceptibility along the ab plane is lower than along the c axis [see inset in Fig. 2(a)]. The crystal and magnetic structures suggest that the easy axis for AFM order lies in the ab plane [2,4]. The susceptibility cusp at $T_N = 110$ K for $x = 0$ indicates that the canted moments in successive layers interact antiferromagnetically. The enhanced distortions in Ir-doped compounds $CaRu_{1-x}Ir_xO_4$ having larger c/a ratios and smaller Ru/Ir-O1-Ru/Ir bond angles further reduce the symmetry and enhance the DM interaction. In contrast to the parent compound Ca_2RuO_4, the interlayer interaction in Ir-doped compounds drives the weak FM behavior observed along the c axis (see Figs. 2 and 3). Figure 2(d) shows a schematic picture of the moment configuration of $CaRu_{1-x}Ir_xO_4$. The net moments along the c axis for individual layers exhibit FM coupling due to canting. It is remarkable that the interlayer coupling changes from AFM coupling for the parent compound Ca_2RuO_4 to FM coupling for Ir-doped compounds.

Indeed, the evolution of the magnetic behavior is remarkably consistent with a theoretical proposal for the iridates that suggests an increased c/a ratio tends to result in a spin-flop transition to a collinear magnetic order along the c axis due to a strong magnetoelastic coupling [30]. That the increase in T_{N2} closely tracks the decrease in the Ir/Ru-O1-Ir/Ru bond angle Θ also manifests the strong magnetoelastic coupling [Fig. 1(b)] Ca_2RuO_4.

It is now recognized that the $5d$-based iridates have strong SOC that competes vigorously with Coulomb interactions, noncubic crystalline electric fields, and other relevant energies, leading to the $J_{\rm eff} = 1/2$ state [17–21]. One profound result of this competition is that $5d$ iridates exhibit complex magnetic states with high critical temperatures, such as Sr_2IrO_4 ($T_N = 240$ K) [22], $Sr_3Ir_2O_7$ ($T_N = 285$ K) [31,32], and $BaIrO_3$ ($T_C = 183$ K) [33,34]. It is established that the magnetic moment and ordering temperature are closely associated with the Ir-O-Ir bond angle Θ [35]. In particular, a recent study reveals that there is a perfect locking between the octahedral rotation and also magnetic moment canting angles that can persist even in the presence of large noncubic local distortions [35,36]. Since Ir doping further reduces Θ, it is not surprising that T_{N2} steadily rises with x, as shown in Figs. 3(a) and 3(b); T_{N2} reaches 210 K for 65% of Ir doping, and would approach an even higher temperature for 100% of Ir doping or Ca_2IrO_4 according to the upward trajectory in Fig. 3(c) should perovskitelike Ca_2IrO_4 exist.

The temperature dependence of the electrical resistivity $\rho(T)$ of $CaRu_{1-x}Ir_xO_4$ is shown in Fig. 4. It is clear that the metal-insulator transition increases from $T_{\rm MI} = 357$ K for $x = 0$ to $T_{\rm MI} = 369$ K for $x = 0.016$, and $T_{\rm MI} = 384$ K for $x = 0.03$, beyond which it is no longer well defined. (It is noted that the slope of the resistivity above $T_{\rm MI}$ is still slightly negative. The magnitude is a few orders of magnitude smaller and the temperature dependence is much weaker compared

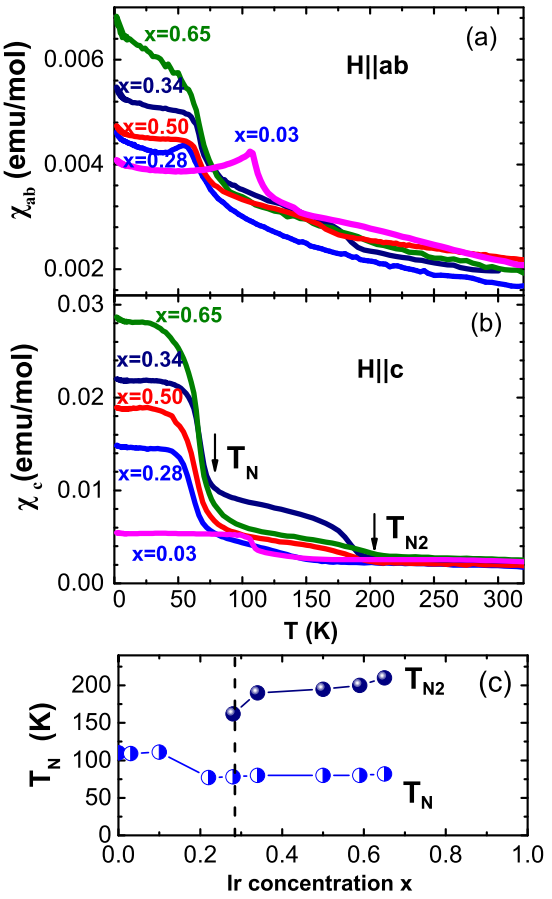

FIG. 3. (Color online) Representative magnetic susceptibilities $\chi(T)$ in the ab plane (a) and along the c axis (b) after field cooling in an applied field $\mu_0 H = 0.1$ T for $CaRu_{1-x}Ir_xO_4$ with $x = 0.03$, 0.28, 0.34, 0.50, and 0.65; the Ir concentration x dependence of Neél temperature T_N and T_{N2}. (c). The data are derived from $\chi(T)$ data for field along the c axis.

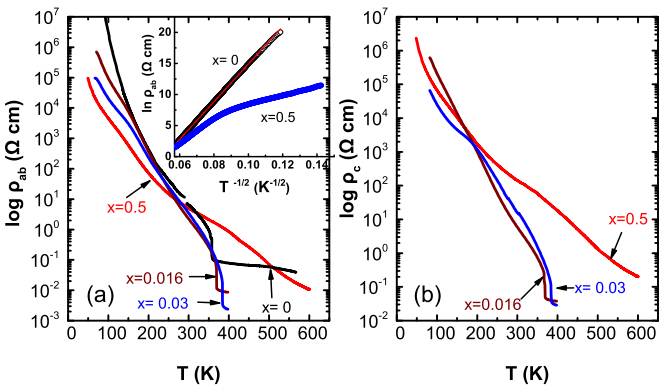

FIG. 4. (Color online) Temperature dependence of the resistivity $\rho(T)$ in the ab plane (a) and along the c axis (b) for representative compositions $x = 0$, 0.016, 0.03, and 0.5. The inset in (a) illustrates variable-range hopping (VRH) in a plot of $\ln\rho_a$ vs $T^{-1/2}$ for $x = 0$ and 0.50.

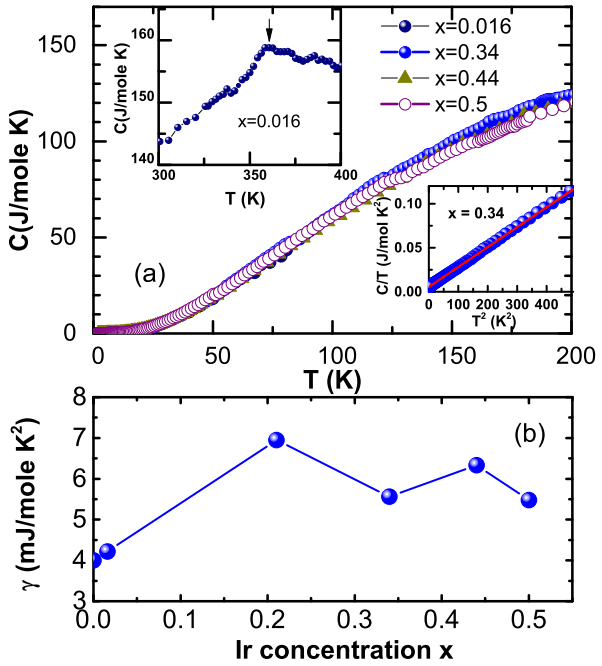

FIG. 5. (Color online) (a) Specific heat $C(T)$ vs T, and (b) Sommerfeld coefficient γ vs x, for $CaRu_{1-x}Ir_xO_4$. The upper inset in (a) shows the anomaly around the metal-insulator transition for $x = 0.016$; the lower inset in (a) shows the fitting results for $C(T)/T$ vs T^2 for a representative $x = 0.34$.

to those below T_{MI}; thus T_{MI} qualifies for a metal-insulator transition.) The increase in T_{MI} closely tracks the enhanced distortions of the Ru/IrO_6 octahedra with reduced Ru/Ir-O1-Ru/Ir bond angle Θ. This behavior contrasts with that of a $3d$ transition-metal ion M (Cr, Mn, Fe) that weakens the orthorhombic distortions, thus, the insulating state [12,13]. The resistivity data over the interval $220 < T < 290$ K fit an activated behavior with a gap of about 0.40 eV for $x = 0$, and 0.28 eV for the Ir-doped crystals. Variable-range hopping (VRH) model [$\rho \sim \exp(1/T)^{1/2}$] fits were more successful for $x = 0$, suggesting Anderson localization is relevant in the parent compound. However, VRH fails to describe the resistivity of Ir-doped crystals.

The heat capacity $C(T)$ data for $0.016 \leqslant x \leqslant 0.65$ show weak or no anomaly at T_N and T_{N2}, while the anomaly around T_{MI} for $x = 0.016$ confirms that the metal-insulator transition involves a structural phase transition between the high-T tetragonal to low-T orthorhombic distortion [12,13], as shown in Fig. 5(a). Interestingly, the heat capacity of Sr_2IrO_4 also shows no corresponding anomaly at the magnetic ordering temperature 240 K, which is one of its signature features of the $J_{eff} = 1/2$ insulator [32]. Fitting the data to $C(T) = \gamma T + \beta T^3$ for $1.7 < T < 20$ K yields the Sommerfeld coefficient γ for the electronic contribution to $C(T)$, which serves as a measure of the electronic density of states at the Fermi level, $N(E_F)$ and the effective mass of the carriers. There is no substantial increase of γ with Ir concentration [Fig. 5(b)].

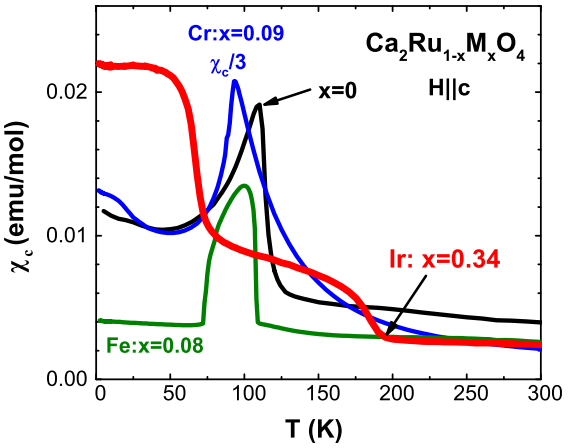

FIG. 6. (Color online) The c-axis magnetic susceptibility along the c axis as a function of temperature for some representative $3d$-element and Ir-doped $Ca_2Ru_{1-x}M_xO_4$ compounds including the parent compound Ca_2RuO_4.

The small values of γ are consistent with the low electrical conductivity observed at low temperatures. The slight increase in γ with increasing x results from the moderate drop in activation gap for Ir-doped compounds.

IV. CONCLUSIONS

The substitution of Ir for Ru in $CaRuO_4$ enhances the SOC and intensifies the distortions of the Ru/IrO_6 octahedra. As a result, the metal-insulator transition rises and a pronounced weak ferromagnetic behavior occurs, which strengthens with increasing Ir concentration. The Ir-induced ordering temperature T_{N2} reaches 210 K at $x = 0.65$, which is remarkably comparable to 240 K for Sr_2IrO_4 [22], along with the enhanced magnetic anisotropy due to SOC. The increase in both T_{N2} and T_{MI} with increased Ir doping closely follows the enhanced Ru/IrO_6 octahedral rotation or reduced Ru/Ir-O1-Ru/Ir bond angle. More generally, the effect of Ir doping tends to strengthen the coupling between the lattice and magnetic moment whereas a $3d$-element doping readily reduces such a coupling and the orthorhombic distortions, thus suppressing the AFM and insulating states and causing the unusual negative volume expansion as well. For comparison and contrast, the magnetic susceptibility for some representative $3d$-element and Ir-doped Ca_2RuO_4 samples is illustrated in Fig. 6, where Cr or Fe doping suppresses T_N whereas Ir doping induces a high-temperature T_{N2}. The sharp contrast highlights a strong magnetoelastic coupling or locking between the octahedral rotation and magnetic moment canting angles, a pronounced characteristic of the SOC-driven iridates such as Sr_2IrO_4, $Sr_3Ir_2O_7$, and $BaIrO_3$ [17,22,31,33,35,36].

ACKNOWLEDGMENT

This work was supported by the National Science Foundation via Grant No. DMR-1265162 and China Scholarship Council (J.C.W.).

[1] Y. Maeno, H. Hashimoto, K. Yoshida, S. Nishizaki, T. Fujita, J. G. Bednorz, and F. Lichtenberg, Nature **372**, 532 (1994).

[2] G. Cao, S. McCall, M. Shepard, J. E. Crow, and R. P. Guertin, Phys. Rev. B **56**, R2916 (1997).

[3] C. S. Alexander, G. Cao, V. Dobrosavljevic, S. McCall, J. E. Crow, E. Lochner, and R. P. Guertin, Phys. Rev. B **60**, R8422 (1999).
[4] M. Braden, G. André, S. Nakatsuji, and Y. Maeno, Phys. Rev. B **58**, 847 (1998).
[5] M. A. Carpenter and C. J. Howard, Acta Crystallogr., Sec. B **65**, 134 (2009).
[6] G. Cao, S. McCall, V. Dobrosavljevic, C. S. Alexander, J. E. Crow, and R. P. Guertin, Phys. Rev. B **61**, R5053 (2000).
[7] S. Nakatsuji and Y. Maeno, Phys. Rev. Lett. **84**, 2666 (2000).
[8] C. S. Snow, S. L. Cooper, G. Cao, J. E. Crow, H. Fukazawa, S. Nakatsuji, and Y. Maeno, Phys. Rev. Lett. **89**, 226401 (2002).
[9] T. Mizokawa, L. H. Tjeng, G. A. Sawatzky, G. Ghiringhelli, O. Tjernberg, N. B. Brookes, H. Fukazawa, S. Nakatsuji, and Y. Maeno, Phys. Rev. Lett. **87**, 077202 (2001).
[10] J. S. Lee, Y. S. Lee, T. W. Noh, S. J. Oh, J. Yu, S. Nakatsuji, H. Fukazawa, and Y. Maeno, Phys Rev. Lett. **89**, 257402 (2002).
[11] J. H. Jung, Z. Fang, J. P. He, Y. Kaneko, Y. Okimoto, and Y. Tokura, Phys. Rev. Lett. **91**, 056403 (2003).
[12] T. F. Qi, O. B. Korneta, S. Parkin, L. E. De Long, P. Schlottmann, and G. Cao, Phys. Rev. Lett. **105**, 177203 (2010).
[13] T. F. Qi, O. B. Korneta, S. Parkin, J. Hu, and G. Cao, Phys. Rev. B **85**, 165143 (2012).
[14] T. F. Qi, M. Ge, O. B. Korneta, S. Parkin, L. E. De Long, and G. Cao, J Solid State Chem. **184**, 893 (2011).
[15] J. C. Wang, J. Terzic, T. F. Qi, F. Ye, S. J. Yuan, S. Aswartham, S. V. Streltsov, D. I. Khomskii, R. K. Kaul, and G. Cao, Phys. Rev. B **90**, 161110 (2014).
[16] G. Cao, T. F. Qi, L. Li, J. Terzic, S. J. Yuan, L. E. DeLong, G. Murthy, and R. K. Kaul, Phys. Rev. Lett. **112**, 056402 (2014).
[17] G. Cao and L. E. DeLong, in *Frontiers of 4d- and 5d-Transition Metal Oxides* (World Scientific, Singapore, 2013).
[18] B. J. Kim, H. Jin, S. J. Moon, J.-Y. Kim, B.-G. Park, C. S. Leem, J. Yu, T. W. Noh, C. Kim, S.-J. Oh, J.-H. Park, V. Durairaj, G. Cao, and E. Rotenberg, Phys. Rev. Lett. **101**, 076402 (2008).
[19] B. J. Kim, H. Ohsumi, T. Komesu, S. Sakai, T. Morita, H. Takagi, and T. Arima, Science **323**, 1329 (2009).
[20] O. B. Korneta, S. Chikara, S. Parkin, L. E. DeLong, P. Schlottmann, and G. Cao, Phys. Rev. B **81**, 045101 (2010).
[21] T. F. Qi, O. B. Korneta, L. Li, K. Butrouna, V. S. Cao, X. Wan, P. Schlottmann, R. K. Kaul, and G. Cao, Phys. Rev. B **86**, 125105 (2012).
[22] G. Cao, J. Bolivar, S. McCall, J. E. Crow, and R. P. Guertin, Phys. Rev. B **57**, R11039 (1998).
[23] G. Cao, S. McCall, J. E. Crow, and R. P. Guertin, Phys. Rev. Lett. **78**, 1751 (1997).
[24] G. Sheldrick, Acta Crystallogr., Sect. A **64**, 112 (2008).
[25] See Supplemental Material at http://link.aps.org/supplemental/10.1103/PhysRevB.92.024425 for substantial information on crystal refinements.
[26] T. Moriya, Phys. Rev. Lett. **4**, 228 (1960).
[27] I. Dzyaloshinsky, J Phys Chem. Solids **4**, 241 (1958).
[28] S. J. Yuan, L. Li, T. F. Qi, L. E. DeLong, and G. Cao, Phys Rev. B **88**, 024413 (2013).
[29] S. Nakatsuji, S.-i. Ikeda, and Y. Maeno, J Phys. Soc. Jpn. **66**, 1868 (1997).
[30] G. Jackeli and G. Khaliullin, Phys Rev Lett. **102**, 017205 (2009).
[31] G. Cao, Y. Xin, C. S. Alexander, J. E. Crow, P. Schlottmann, M. K. Crawford, R. L. Harlow, and W. Marshall, Phys. Rev. B **66**, 214412 (2002).
[32] L. Li, P. P. Kong, T. F. Qi, C. Q. Jin, S. J. Yuan, L. E. DeLong, P. Schlottmann, and G. Cao, Phys Rev. B **87**, 235127 (2013).
[33] G. Cao, J. E. Crow, R. P. Guertin, P. F. Henning, C. C. Homes, M. Strongin, D. N. Basov, and E. Lochner, Solid State Commun. **113**, 657 (2000).
[34] M. L. Brooks, S. J. Blundell, T. Lancaster, W. Hayes, F. L. Pratt, P. P. C. Frampton, and P. D. Battle, Phys Rev. B **71**, 220411 (2005).
[35] F. Ye, S. Chi, B. C. Chakoumakos, J. A. Fernandez-Baca, T. Qi, and G. Cao, Phys Rev. B **87**, 140406 (2013).
[36] D. H. Torchinsky, H. Chu, L. Zhao, N. B. Perkins, Y. Sizyuk, T. Qi, G. Cao, and D. Hsieh, Phys Rev. Lett. **114**, 096404 (2015).